mutants, one representative each of the suppressed and enhanced *bri1-301* transgenic plants containing the *35S-BIN2* transgene. Using a full-length *BIN2* cDNA as a probe, we observed a ~50-fold accumulation of *BIN2* transcripts in the enhanced *bri1-301* line compared with the wild-type control (Fig. 3D). However, no difference in hybridization signal was observed between the suppressed line and the other three tested plants, most likely due to cross-hybridization of the full-length *BIN2* probe with other *Arabidopsis GSK3/SHAGGY-like* genes. To see if the suppressed *bri1-301* line accumulated fewer *BIN2* messages, we used a gene-specific probe corresponding to the 3′-untranslated region of the *BIN2* cDNA that was not included in the *35S-BIN2* transgene. As shown in Fig. 3D, the suppressed line accumulated ~20% of the amount of *BIN2* transcripts in the wild-type control. Because such a cosuppressed line is equivalent to a reduction-of-function *bin2* mutant, this result provides a further support for BIN2 being a negative regulator in a BRI1-mediated BR signaling pathway.

Our results indicate that a GSK/SHAGGY-like kinase plays an important role in a steroid signal transduction pathway. In animals, GSK3/SHAGGY is a constitutively active kinase that negatively regulates a variety of substrates by phosphorylation, and the inhibition of its kinase activity constitutes a key event in many signal transduction pathways (*13*). It is well established that GSK3/SHAGGY kinase itself is negatively regulated by protein phosphorylation or protein-protein interaction in response to a variety of stimuli (*13*). If BIN2 functions as a negative regulator in BR signaling, a crucial step in this signal transduction pathway would be to inhibit the BIN2 kinase activity in response to BR signals, which are thought to be perceived by BRI1, a leucine-rich-repeat–receptor–like kinase (*5*–*8*). Thus, it is quite tempting to speculate that BRI1 might be one of the upstream kinases that could phosphorylate and inactivate BIN2 to relieve its inhibitory effect on downstream BR signaling components. However, repeated experiments using yeast two-hybrid analysis and in vitro protein interaction assay failed to demonstrate a direct physical interaction between BRI1 and BIN2, suggesting the existence of additional regulators that are involved in suppressing BIN2 activity. We hypothesize that, in the absence of BRs, BIN2 is a constitutively active kinase that can phosphorylate and inactivate positive BR signaling proteins to block BR signal transduction. The identification of upstream regulators and downstream targets of the BIN2 kinase is crucial to understand the molecular mechanisms of steroid signaling in plants.

References and Notes

1. S. D. Clouse, J. Sasse, *Annu. Rev. Plant Mol. Biol. Plant Physiol.* **49**, 427 (1998).
2. J. Li, P. Nagpal, V. Vitart, T. C. McMorris, J. Chory, *Science* **272**, 398 (1996).
3. M. Szekeres *et al.*, *Cell* **85**, 171 (1996).
4. S. D. Clouse, M. Langford, T. C. McMorris, *Plant Physiol.* **111**, 671 (1996).
5. J. Li, J. Chory, *Cell* **90**, 929 (1997).
6. D. M. Friedrichsen, C. A. Joazeiro, J. Li, T. Hunter, J. Chory, *Plant Physiol.* **123**, 1247 (2000).
7. Z. He *et al.*, *Science* **288**, 2360 (2000).
8. Z.-Y. Wang, H. Seto, S. Fujioka, S. Yoshida, J. Chory, *Nature* **410**, 380 (2001).
9. J. Li, K. H. Nam, D. Vafeados, J. Chory, *Plant Physiol.* **127**, 14-22 (2001).
10. M. C. Domelas, P. E. Wittich, I. R. von Recklinghausen, A. A. M. van Lammeren, M. Kreis, *Plant Mol. Biol.* **39**, 137 (1999).
11. J. R. Woodgett, *EMBO J.* **9**, 2431 (1990).
12. E. Siegfried, L. A. Perkins, T. M. Capaci, N. Perrimon, *Nature* **345**, 825 (1990).
13. J. R. Woodgett, *Science's STKE* (2001), http://stke.sciencemag.org/cgi/content/full/OC_sigtrans; 2001/100/re12.
14. M. C. Dornelas, B. Lejeune, M. Dron, M. Kreis, *Gene* **212**, 249 (1998).
15. H. L. Piao *et al.*, *Plant Physiol.* **119**, 1527 (1999).
16. C. Jonak, D. Beisteiner, J. Beyerly, H. Hirt, *Plant Cell* **12**, 1467 (2000).
17. M. C. Dornelas, A. A. van Lammeren, M. Kreis, *Plant J.* **21**, 419 (2000).
18. A 6.2-kb Spe I fragment was cloned from BAC F28A21 into the pPZP212 vector (*23*). To create the *bin2-1* mutation, two complementary primers (CACCAACTCGAAAAGAAATCCGTTG and CAACGGATTTCTTTTCGAGTTGGTG) were used for site-directed mutagenesis using the Stratagene QuikChange site-directed mutagenesis kit. The primer set (CCGTGGCGA TAAGGAAGGTTTTGC and GCAAAACCTTCCT TATCGCCACGG) was used to create K69R mutation with DNAs of wild-type and the *bin2-1*–mutated *BIN2* genomic constructs.
19. Single letter abbreviations for amino acid residues: A, Ala; C, Cys; D, Asp; E, Glu; F, Phe; G, Gly; H, His; I, Ile; K, Lys; L, Leu; M, Met; N, Asn; P, Pro; Q, Gln; R, Arg; S, Ser; T, Thr; V, Val; W, Trp; and Y, Tyr.
20. S. B. Pierce, D. Kimelman, *Development* **121**, 755 (1995).
21. To express BIN2 protein in *E. coli*, a BIN2 cDNA was cloned into the pGEX-KG vector (*24*), and the resulting plasmid was used to create the *bin2-1*, K69R, or *bin2-1*, K69R double mutation, as described above. The induction and protein purification was carried out according to a published protocol (*24*). The transphosphorylation activity of each GST-BIN2 fusion protein was assayed as described (*25*) by using the CREB phosphopeptide [KRREILSRRPS(p)YR, New England Biolab] as a substrate.
22. Jiayang Li, unpublished data.
23. P. Hajdukiewicz, Z. Svab, P. Maliga, *Plant Mol. Biol.* **25**, 989 (1994).
24. K. Guan, J. E. Dixon, *Anal. Biochem.* **192**, 262 (1991).
25. S. Frame, P. Cohen, R. M. Biondi, *Mol. Cell* **7**, 1321 (2001).
26. T. Mozo *et al.*, *Nature Genet.* **22**, 271 (1999).

27. We thank K. Cadigan, J. Chory, S. Clark, and J. Schiefelbein for their critical comments, members of Li lab for helpful discussions, and W. Chiang for technical assistance. We are grateful to Jiayang Li (The Institute of Genetics, The Chinese Academy of Sciences) for the *bri1-301* mutant and the *Arabidopsis* Biological Resource Center for various plasmids, BAC clones, and *Arabidopsis* cDNA libraries. This work was supported in part by a University of Michigan Rackham Faculty Research award, a Michigan Memorial Phoenix Project grant, and an NIH grant (GM60519) to J.L.

27 August 2001; accepted 7 January 2002

Requirement of the Activation-Induced Deaminase (*AID*) Gene for Immunoglobulin Gene Conversion

Hiroshi Arakawa, Jessica Hauschild, Jean-Marie Buerstedde*

Three phenotypically distinct processes—somatic hypermutation, gene conversion, and switch recombination—remodel the functionally rearranged immunoglobulin (Ig) loci in B cells. Somatic hypermutation and switch recombination have recently been shown to depend on the activation-induced deaminase (*AID*) gene product. Here, we show that the disruption of the *AID* gene in the chicken B cell line DT40 completely blocks Ig gene conversion and that this block can be complemented by reintroduction of the *AID* complementary DNA. This demonstrates that the *AID* master gene controls all B cell–specific modifications of vertebrate Ig genes.

The formation of a large antigen receptor repertoire by DNA rearrangement and hypermutation is unique to the immune system. Early lymphocytes first assemble their antigen receptor genes from different V, D, and J segments by site-specific V(D)J recombination. B cells then further modify the rearranged V segments by untemplated hypermutation (*1*) or pseudogene templated gene conversion (*2*). Some species (such as sheep) exclusively use somatic hypermutation for V segment diversification, whereas others (such as chickens, rabbits, cattle, and pigs) rely predominantly on Ig gene conversion (*3*). Concomitant with antigen stimulation, the Ig heavy chain locus is further reshuffled by

Department of Cellular Immunology, Heinrich-Pette-Institute, Martinistrasse 52, 20251 Hamburg, Germany.

*To whom correspondence should be addressed. E-mail: buersted@hpi.uni-hamburg.de

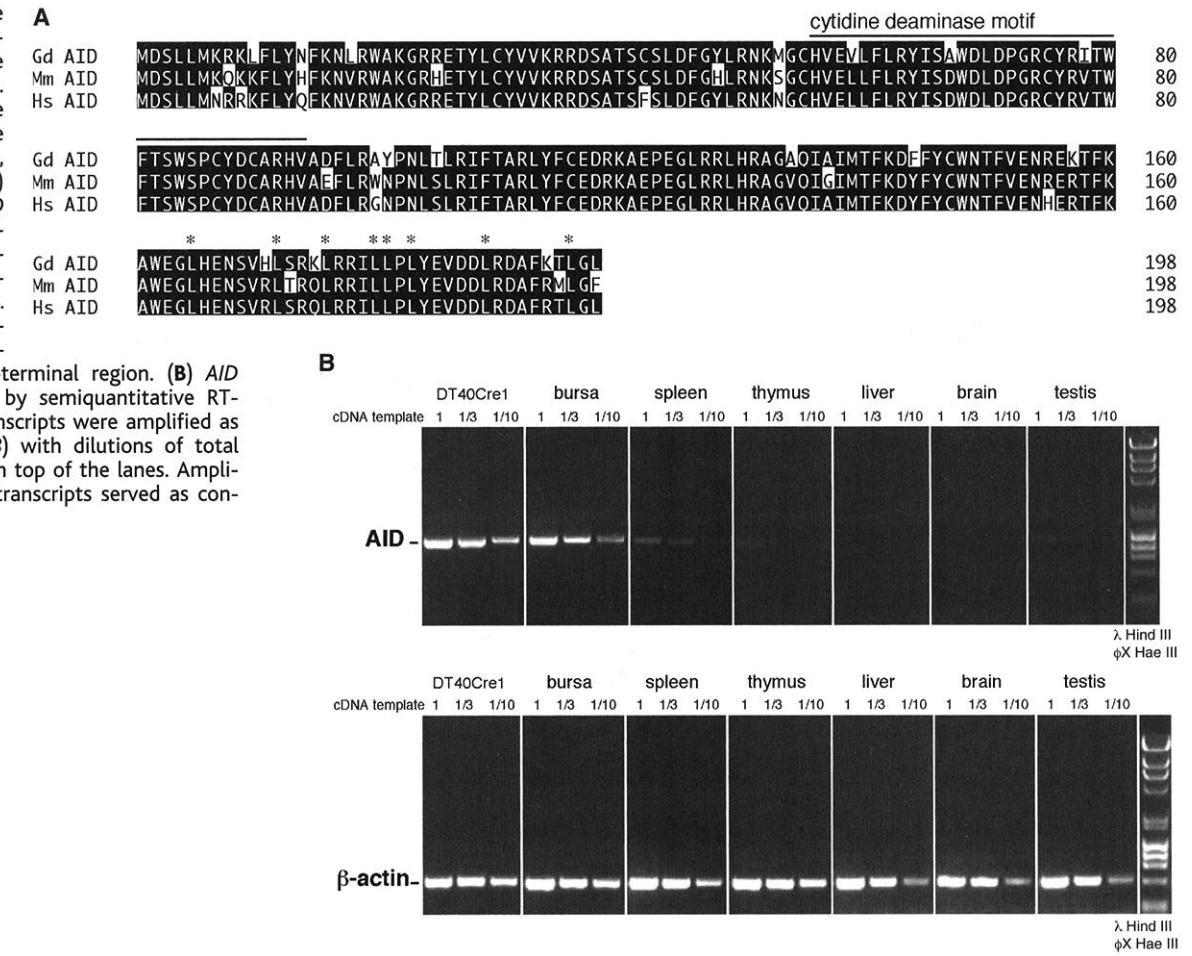

Fig. 1. Sequence conservation and expression of the chicken *AID* gene. (**A**) Alignment of the chicken (Gd), mouse (Mm) (NM_009645), and human (Hs) (NM_020661) *AID* amino acid sequences. The conserved cytidine deaminase motif is marked by a line. Asterisks denote conserved leucine residues in the COOH-terminal region. (**B**) *AID* expression analyzed by semiquantitative RT-PCR. *AID* specific transcripts were amplified as described in (*17*, *18*) with dilutions of total cDNA as indicated on top of the lanes. Amplifications of β-actin transcripts served as controls (*18*).

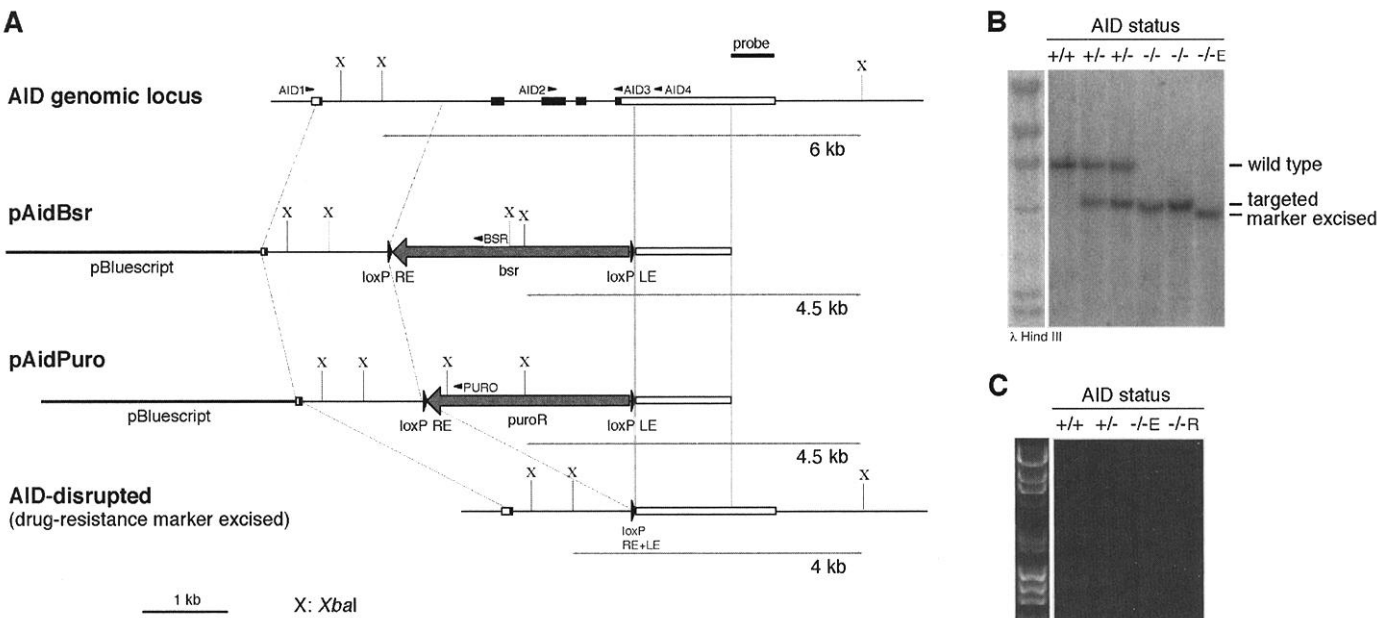

Fig. 2. Disruption of the chicken *AID* gene (*20*, *21*). (**A**) A physical map of the *AID* locus, the two knockout constructs, and the targeted loci. Open boxes represent transcribed 5′ and 3′ untranslated regions. Solid boxes represent coding regions. The positions of primers for RT-PCR and the identification of targeted integration events are indicated by arrowheads. (**B**) Southern blot analysis of wild-type and transfected clones using theprobe shown in (A) after Xba I digestion. The wild-type locus hybridizes as a 6-kb fragment, whereas the targeted locus hybridizes as a 4.5-kb fragment and a 4-kb fragment before and after removal of the drug resistance marker cassettes, respectively. (**C**) *AID* expression. Transcripts of *AID* were amplified by RT-PCR (*17*, *18*) to verify the gene disruptions and the complementation.

switch recombination to yield different Ig isotypes (*4*).

It was reported recently that mutations of the so-called *AID* gene, which is induced by B cell stimulation and is homologous to the cytidine deaminase *APOBEC-1* gene (*5*), abolish switch recombination and severely reduce somatic hypermutation in mice (*6*) and humans (*7*). It is speculated that the AID protein acts by sequence-specific mRNA editing in a manner similar to that of the APOBEC-1 protein. The AID mutant phenotypes raise the question whether *AID* might regulate Ig gene conversion as well. The best characterized model for Ig gene conversion is the chicken Ig light chain locus, for which all V pseudogenes have been sequenced (*2*).

To investigate the role of *AID* in Ig gene conversion, we cloned the chicken *AID* homolog and disrupted it in the bursal B cell DT40 cell line, where light chain gene conversion is preserved (*8*). An expressed sequence tag (EST) (riken1_1b7r1) of the likely 5′ end of the chicken *AID* cDNA was identified in the bursal EST database (*9*) and extended by primer walk. The corresponding cDNA insert contains an open reading frame of 198 amino acids with over 85% identity to the murine and human *AID* sequence (Fig. 1A). Expression of this bonafide chicken *AID* homolog was analyzed by semiquantitative reverse transcription–polymerase chain reaction (RT-PCR) in different cell types (Fig. 1B). *AID* is highly expressed in the bursa of Fabricius and DT40 cells; weakly expressed in the spleen, thymus, and testis; but no expression is detected in the liver or brain. Because the bursa of Fabricius is the main site of Ig gene conversion, this expression pattern is compatible with a role for *AID* in this process. Two *AID* knockout constructs (pAidBsr and pAidPuro) were made by cloning genomic fragments from the 5′ end and the 3′ untranslated region of the *AID* locus upstream and downstream of loxP-flanked drug-resistance markers (Fig. 2A). Targeted integration of these constructs deletes the *AID* coding region from the third codon to the end, resulting in an *AID* null mutation.

Table 1. Percentages of events falling into the sIgM(+) gates for individual subclones.

DT40IgL$^-$	DT40Cre1	AID$^{+/-}$	AID$^{-/E}$	AID$^{-/-R}$
0.06%	0.85%	0.26%	0.22%	4.22%
0.09%	1.48%	0.20%	0.10%	2.14%
0.30%	1.95%	0.04%	0.14%	1.74%
0.12%	36.54%	0.07%	0.13%	1.42%
0.18%	1.25%	0.09%	0.20%	32.92%
0.58%	0.18%	0.12%	0.12%	0.74%
0.11%	1.52%	0.21%	0.13%	1.20%
0.14%	33.07%	0.14%	0.13%	4.98%
0.34%	10.35%	0.07%	0.12%	0.17%
0.09%	3.67%	0.17%	0.21%	47.05%
0.04%	0.47%	0.12%	0.09%	1.06%
0.11%	0.25%	0.03%	0.10%	0.54%
0.10%	3.98%	0.15%	0.12%	1.17%
0.11%	3.92%	0.10%	0.13%	0.90%
0.10%	1.71%	0.12%	0.13%	2.12%
0.05%	5.65%	0.29%	0.33%	3.05%
0.10%	0.36%	0.11%	0.06%	35.22%
0.07%	0.55%	0.03%	0.10%	2.49%
0.07%	0.98%	0.34%	0.12%	13.98%
0.12%	60.17%	0.07%	0.31%	18.58%
0.03%	10.44%	0.14%	0.10%	3.70%
0.06%	0.82%	0.05%	0.08%	5.43%
0.05%	3.42%	0.05%	0.37%	0.43%
0.10%	2.72%	0.03%	0.10%	2.94%
0.31%	5.83%	0.12%	0.17%	3.09%
0.13%	1.18%	0.30%	0.22%	1.20%
0.19%	5.49%	0.14%	0.28%	3.84%
0.07%	1.11%	0.31%	0.07%	68.68%
0.06%	1.77%	0.17%	0.07%	4.14%
0.05%	21.51%	0.16%	0.07%	21.58%
0.07%	1.65%	0.22%	0.24%	27.69%
0.07%	1.61%	0.10%	0.17%	2.78%
0.08%	13.05%	0.21%	0.04%	2.16%
0.09%	4.80%	0.17%	0.13%	0.14%
0.17%	1.97%	0.11%	0.25%	2.45%
0.05%	4.62%	0.14%	0.12%	13.83%
0.30%	1.97%	0.22%	0.31%	78.37%
0.08%	4.43%	0.16%	0.12%	2.68%
0.10%	5.64%	0.13%	0.14%	2.23%
0.12%	0.70%	0.13%	0.07%	2.84%
0.10%	1.35%	0.13%	0.07%	0.88%
0.07%	2.85%	0.11%	0.11%	0.59%
0.25%	0.08%	0.15%	0.11%	0.74%
0.00%	5.81%	0.13%	0.14%	5.29%
0.05%	7.27%	0.21%	0.07%	6.00%
0.13%		0.15%	0.13%	0.88%
0.00%		1.75%	0.16%	2.97%
0.09%		9.44%	0.02%	
0.12%	6.24%	0.37%	0.14%	9.43%
(0.00%)	(6.12%)	(0.25%)	(0.02%)	(9.31%)

Ig gene conversion rates can be measured easily by quantifying cell surface(s) IgM reversion rates in the predominately sIgM(–) CL18 cell line (*8*). This spontaneous DT40 variant has a frameshift in its rearranged V segment, which can be repaired by homologous pseudogene sequences (Fig. 3A). Because CL18 shows rather low light chain conversion frequencies, a v-myb transfectant of CL18, which has five times higher rates of sIgM reversion (*10*), was used. This clone, DT40Cre1, also contains a transfected *MerCreMer* recombinase gene, which can be induced to excise loxP-flanked cassettes (*11*). After transfection of pAidBsr into DT40Cre1, a heterozygous *AID* clone was identified (DT40AID$^{+/-}$) which was subsequently transfected by pAidPuro to produce a homozygous *AID* knockout clone (DT40AID$^{-/-}$) (Fig. 2A). Both the blasticidin and the puromycin resistance markers were then removed from DT40AID$^{-/-}$ by tamoxifen induction of the MerCreMer recombinase (*12*), yielding the clone DT40AID$^{-/-E}$. The disruption of *AID* in DT40AID$^{+/-}$ and DT40AID$^{-/-}$, and the excision of the resistance marker cassettes in DT40AID$^{-/-E}$, were confirmed by Southern blot analysis (Fig. 2, A and B). To reconstitute the *AID* disruption, DT40AID$^{-/-E}$ was transfected by an *AID* expression vector in which the *AID* cDNA and the puromycin gene were under the control of the β-actin promoter and were flanked by loxP sites. One of eight stable puromycin resistant transfectants (DT40AID$^{-/-R}$) expressed the *AID* cDNA (Fig. 2C).

To quantify the Ig gene conversion rates, 48 subclones of the wild-type positive control and the *AID* mutant clones were analyzed for sIgM expression by fluorescence-activated cell sorting (FACS) after 18 days of being cultured. Subclones of the stable sIgM(–) light chain knockout DT40IgL$^-$ were included as negative controls. Representative FACS anti-IgM stainings of subclones are shown in Fig. 3B, and the average number of events in the positive gate from the 48 subclones is displayed in Fig. 3C

(the individual clone measurements are in Table 1). This analysis indicates that the disruption of a single *AID* allele reduces the sIgM reversion rate of DT40AID$^{+/-}$ by more than 10 times, although the reversion is not completely blocked, because at least 2 of the 48 DT40AID$^{+/-}$ subclones showed distinct sIgM(+) populations. The disruption of both *AID* alleles in DT40AID$^{-/-E}$ reduces the reversion frequency by at least 100 times. Reexpression of the *AID* gene in DT40AID$^{-/-R}$ increases the frequency of sIgM reversion above that

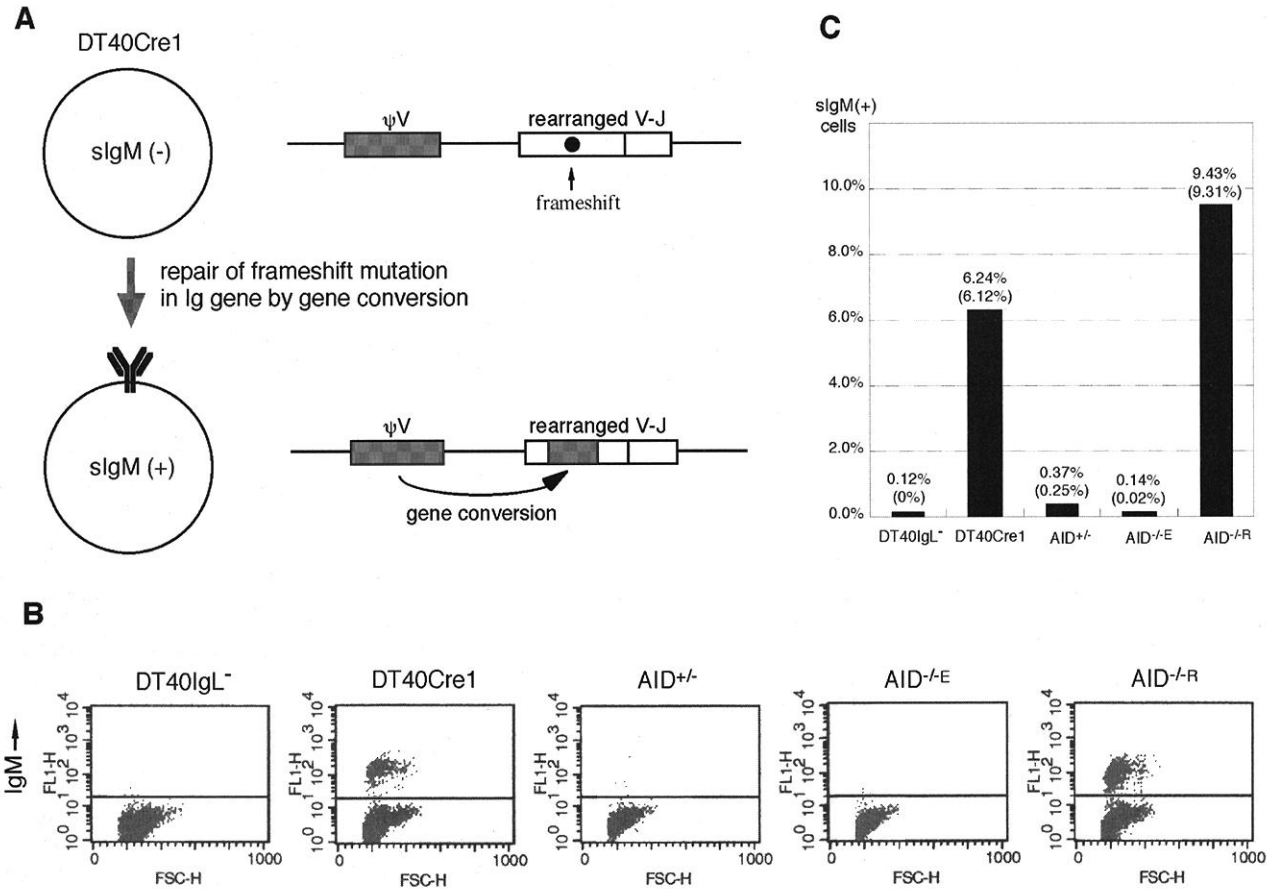

Fig. 3. Ig gene conversion quantified by sIgM expression. (**A**) Principle of the Ig reversion assay. The predominantly sIgM(–) DT40Cre1 clone contains a frameshift in its rearranged V segments, which can be repaired by pseudogene templated conversion events. The rate of Ig gene conversion can be measured in subclones by FACS analysis after staining for sIgM. (**B**) FACS profiles of representative subclones (*22*). (**C**) Average percentages of events falling into the sIgM(+) gates. Forty-eight subclones of each clone were analyzed (*22*). The measurements for individual subclones are shown in Table 1. The percentages in brackets are the values after subtraction of the background. (**D**) Sequences of the CDR1 regions from the rearranged V segments of DT40 Cre1 and AID$^{-/-E}$ clones 6 weeks after subcloning (*23*). Dashes indicate nucleotides identical to the sequence of DT40 Cre1 sIgM(–), and brackets mark the borders of deletions. Gene conversion tracts are underlined and annotated with the name of the likely pseudogene donor.

D

	21 22 23 24 25 26 (CDR1) 27 28	number of sequences
germline	TCC GGG GAT AGC AGC TAC ... ... TAT GGC	
DT40 Cre1 sIgM (-)	TCC GGG GGT GGC AGC TAC G GCT GGA AGT TAC TAT TAT GGC	
DT40 Cre1 6 week culture	--- --- --- -A- --- AG- TA- --- --- --- --- --- --- (ψV4)	32
	--- --- --- --- --- --T --- --- --- --- --- --- --- (ψV8)	14
	--- --- --- --- --- --- I --- --- -[]CAGT GC- --- --- (ψV11)	2
	--- --- --C A-- TAT AG- [ ] --- --- (ψV14)	2
	--- --- --- --T --- AG- [ ] AG- --C --- --- (ψV5)	2
	--- --- --- A-- --T GG- [ ] -GT GG- --- --- (ψV12)	1
	-GC TCC GGG GGT --- --- --- I AGC A-T G-C -GT GG- --- --- (ψV12)	1
	total	54
AID$^{-/-E}$ 6 week culture	--- --- --- --- --- --- I --- --- --- --- --- --- ---	80
	total	80

measured for the parental DT40Cre1 clone. This strongly suggests that *AID* expression is essential for Ig gene conversion. To increase the sensitivity of the assay, we cultured 24 DT40AID$^{-/-E}$ subclones for 6 weeks in parallel with DT40Cre1 subclones. Whereas, on average, more than 60% of DT40Cre1 cells scored sIgM(+), no sIgM(+) populations were detectable in the DT40AID$^{-/-E}$ subclones.

There remained the possibility that the lack of sIgM(+) cells in the *AID* negative clones was not due to a block of Ig gene conversion but was caused by a lack of Ig light or heavy chain transcription. We therefore confirmed by RT-PCR that the light and heavy chain Ig mRNA was present in the DT40AID$^{-/-}$ cells (*10*). To rule out the possibility that the lack of *AID* expression indirectly affects sIgM expression, we removed the loxP-flanked *AID* expression cassette from a predominantly sIgM(+) DT40AID$^{-/-R}$ subclone by tamoxifen induction. FACS analysis confirmed that the level of sIgM expression in the resulting *AID*$^{-/-}$ subclones was identical to the level of sIgM in wild-type DT40Cre1 sIgM(+) cells. Together, these results indicate that *AID*$^{-/-}$ sIgM(+) cells are viable and that the lack of sIgM reversion in *AID*-negative clones is not caused by a defect in sIgM expression but by inhibition of Ig gene conversion. To confirm by sequence analysis that *AID* disruption prevents gene conversion, we compared the light chain genes of DT40Cre1 and AID$^{-/-E}$ clones 6 weeks after subcloning. The CL18 frameshift was replaced by gene conversion tracts in the majority of wild-type cells, but no evidence for a gene conversion event was found in 80 light chain sequences from *AID*-negative cells (Fig. 3D).

The *AID* disruption in DT40 produces a complete block of Ig gene conversion. We have tested a number of DNA repair and recombination candidate genes over the years, but these mutants either maintain Ig gene conversion at wild-type levels [*RAG-2* (*13*), *MSH4*, *MSH3*, *MSH6*, and *POLλ* (*10*)] or show a modest reduction, most likely due to defects in general homologous recombination [*RAD54* (*14*) and *RAD52* (*10*)]. The abolition of all detectable frameshift repair in the *AID*$^{-/-}$ DT40 mutant is remarkable, because a low level of gene conversion can be easily detected in non–B cell lines if an appropriately designed transgene with a donor and recipient sequence is provided (*15*). The dependence on *AID* expression strongly supports the notion that the repair of the V segment frameshift in DT40 reflects B cell–specific Ig gene conversion. The reduction of Ig gene conversion in the heterozygous clone suggests that *AID* acts in a dose-dependent manner. No clear reduction in somatic hypermutation or switch recombination was reported for the *AID*$^{+/-}$ heterozygous mice (*6*) and human carriers (*7*), although the results of transfection experiments with the CH12F3-2 cell line also suggest a dose-dependent stimulation of switch recombination (*6*).

The *AID*$^{-/-}$ phenotype links Ig gene conversion to the other two *AID*-regulated processes: somatic hypermutation and switch recombination. Although it had been speculated for a long time that Ig gene conversion and somatic hypermutation are related and possibly initiated by the same lesion, the DT40 *AID* mutant provides direct genetic evidence for such a relationship. Because somatic hypermutation and switch recombination can be dissociated in certain cell types, and because DT40 does not seem to undergo switch recombination (*10*), events downstream of the *AID* action must determine which of the three processes are executed. The recent finding that mutations in the *RAD51* homologs *XRCC2* and *XRCC3* activate somatic hypermutation in DT40 (*16*) suggests that the decision between Ig gene conversion and somatic hypermutation is influenced by the availability of a specific homologous recombination pathway.

Table 2. Oligonucleotide primer sequences.

	Sequence
AID1	GTTTCTGTGCACCAGAGGGCTGAACAGTCA
AID2	CTACCGCATCACATGGTTCACCTCCTGGAG
AID3	CCCAGATCTTGCTTGTGAAGTCTTCTTATTGCTG
AID4	CTCCTTTCTTGGCTGGGTGAGAGGTCCATA
AID5	GGGCTCGAGGTCATCTGAGAGAGAGAACCCAGCTGACATGG
AID6	GGGGGATCCGCTTCACAACTTAACAGAGGTAGGTTTCA
AID7	GGGGGATCCGTGAGAGTACTGAACTGAGTCCTGGACAG
AID8	GGGACTAGTCAGTCAACATCAGGCAGGAAGATCTGGTTT
AID9	CCCGCTAGCGCTGACATGGACAGCCTCTTGATGA
ACTIN1	CCCCAAGCTTACTCCCACAGCCAGCCATGG
ACTIN2	GGCTCTAGATAGTCCGTCAGGTCACGGCCA
BSR	CGATTGAAGAACTCATTCCACTCAAATATACCC
PURO	CAGCGCCCGACCGAAAGGAGCGCACGACC
Vλ1	GGGAAGCTTTGGGAAATACTGGTGATAGGTGGAT
C2	CCTCCATTTCTAGACAGCACTTACCTGGACAGCTG
V3	CCTCTCTCCTCTCCCTCTCCAGGTTC

References and Notes

1. J. Jacob, G. Kelsoe, K. Rajewsky, U. Weiss, *Nature* **354**, 389 (1991).
2. C.-A. Reynaud, V. Anquez, H. Grimal, J.-C. Weill, *Cell* **48**, 379 (1987).
3. M. Diaz, M. F. Flajnik, *Immunol. Rev.* **162**, 13 (1998).
4. T. Honjo, T. Kataoka, *Proc. Natl. Acad. Sci. U.S.A.* **75**, 2140 (1978).
5. B. Teng, C. F. Burant, N. O. Davidson, *Science* **260**, 1816 (1993).
6. M. Muramatsu *et al.*, *Cell* **102**, 553 (2000).
7. P. Revy *et al.*, *Cell* **102**, 565 (2000).
8. J.-M. Buerstedde *et al.*, *EMBO J.* **9**, 921 (1990).
9. J.-M. Buerstedde *et al.*, *Nucleic Acids Res.* **30**, 230 (2002).
10. H. Arakawa, J.-M. Buerstedde, unpublished results.
11. H. Arakawa, D. Lodygin, J.-M. Buerstedde, *BMC Biotechnol.* **1**, 7 (2001).
12. Y. Zhang *et al.*, *Nucleic Acids Res.* **24**, 543 (1996).
13. S. Takeda, E. L. Masteller, C. B. Thompson, J.-M. Buerstedde, *Proc. Natl. Acad. Sci. U.S.A.* **89**, 4023 (1992).
14. O. Bezzubova, A. Silbergleit, Y. Yamaguchi-Iwai, S. Takeda, J.-M. Buerstedde, *Cell* **89**, 185 (1997).
15. R. M. Liskay, J. L. Stachelek, *Cell* **35**, 157 (1983)
16. J. E. Sale, D. M. Calandrini, M. Takata, S. Takeda, M. S. Neuberger, *Nature* **412**, 921 (2001).
17. Oligonucleotide primer sequences are shown in Table 2.
18. For RT- and long-range PCR, total RNA was extracted by TRIzol (Gibco BRL), and cDNA was synthesized using SuperScript Preamplification System (Gibco BRL) according to the manufacturer's instructions. Primer pairs AID1/AID4 (Fig. 1B) and AID2/AID3 (Fig. 2C) (*17*) were used for amplification of the *AID* transcript, and primer pair ACTIN1/ACTIN2 was used for amplification of the β-actin transcript. PCR amplification was performed with the Expand Long Template PCR System (Roche) under the following conditions: 2 min of initial incubation at 93°C; 35 cycles consisting of 10 s at 93°C, 30 s at 65°C, and 5 min at 68°C, with 20 s of elongation per cycle; and a final elongation step of 7 min at 68°C. About 6 kb of the *AID* locus were amplified by long-range PCR using the *AID* cDNA–derived primers AID1-AID9. The positions of exons in the locus were characterized by comparing the sizes of the PCR fragments amplified with different primer combinations.
19. H. Arakawa, S. Furusawa, S. Ekino, H. Yamagishi, *EMBO J.* **15**, 2540 (1996).
20. For DT40 cell culture, transfection, and subcloning were done as previously described (*8*, *14*), except that Iscove's Modified Dulbecco's Medium was substituted for RPMI medium, and 700 V instead of 550 V were used on the local GenePulser (Bio-Rad), because this resulted in approximately 50% cell killing.
21. Knockout constructs were generated as follows: Primer combinations AID5/AID6 and AID7/AID8 (*17*) were used to amplify the 5′ and 3′ target sequences of the *AID* knockout constructs, as described (*18*). The 3′ sequence was digested by Bam HI–Spe I and cloned into the Bam HI–Xba I sites of pBluescript KS(+). The 5′ sequence was cloned into the Xho I–Eco RV sites of the resulting plasmid after Xho I–Sca I digestion. This produced a plasmid with a unique Bam HI site between the *AID* target sequences into which the pLoxBsr and the pLoxPuro marker cassettes (*11*) were inserted. The resulting two knockout constructs, pAidBsr and pAidPuro, were linearized by Not I before transfection. The *AID* coding sequence was amplified by primers AID9/AID3 (*17*) using high-fidelity PfuTurbo polymerase (Stratagene). This PCR fragment was digested by Nhe I and Bgl II and cloned into the Nhe I and Bgl II sites of pExpress (*11*). The *AID* coding sequence was verified by sequencing. The Spe I cassette of the pAidExpress plasmid was then cloned into the Nhe I site of pLoxPuro, resulting in the *AID* expression vector pAidExpressPuro. pAidExpressPuro was linearized by Sca I before transfection.
22. Quantification of sIgM expression was done as follows: Forty-eight subclones were obtained from each of the DT40IgL^{-}, DT40Cre1, DT40AID$^{+/-}$, DT40AID$^{-/-E}$, and DT40AID$^{-/-R}$ clones by limiting dilution. Eighteen days after subcloning, all the subclones were stained first with a monoclonal

antibody to chicken Cμ (M1) (Southern Biotechnology Associates, Birmingham, AL) and then with polyclonal fluorescein isothiocyanate–conjugated goat antibodies to mouse IgG $(Fab)_2$ (Sigma). Predominantly sIgM(+) subclones were excluded from the analysis, because they most likely originated from cells that were already sIgM(+) at the time of subcloning.

23. For Ig light chain sequencing, PCR amplification and sequencing of the rearranged light chain V segments were performed as previously described (*19*), except that high-fidelity PfuTurbo polymerase (Stratagene) was used with primer pair Vλ1/Vλ2 for PCR, and primer Vλ3 was used for sequencing (*17*). Only one nucleotide change, which most likely reflects a PCR-introduced artifact, was noticed in the V-J-3′ intron region in a total of 80 0.5-kb-long sequences from $AID^{-/-E}$ cells.

24. We thank M. Reth and T. Brummer for kindly providing the MerCreMer plasmid vector; P. Carninci and Y. Hayashizaki for construction of the riken1 bursal cDNA library; A. Peters and K. Jablonski for excellent technical help; and C. Stocking and J. Löhrer for carefully reading the manuscript. Supported by grant Bu 631/2-1 from the Deutsche Forschungsgemeinshaft, by the European Union Framework V programs "Chicken Image" and "Genetics in a Cell Line," and by Japan Society for the Promotion of Science Postdoctoral Fellowships for Research Abroad.

22 October 2001; accepted 18 December 2001

Capturing Chromosome Conformation

Job Dekker,[1]* Karsten Rippe,[2] Martijn Dekker,[3] Nancy Kleckner[1]

We describe an approach to detect the frequency of interaction between any two genomic loci. Generation of a matrix of interaction frequencies between sites on the same or different chromosomes reveals their relative spatial disposition and provides information about the physical properties of the chromatin fiber. This methodology can be applied to the spatial organization of entire genomes in organisms from bacteria to human. Using the yeast *Saccharomyces cerevisiae*, we could confirm known qualitative features of chromosome organization within the nucleus and dynamic changes in that organization during meiosis. We also analyzed yeast chromosome III at the G_1 stage of the cell cycle. We found that chromatin is highly flexible throughout. Furthermore, functionally distinct AT- and GC-rich domains were found to exhibit different conformations, and a population-average 3D model of chromosome III could be determined. Chromosome III emerges as a contorted ring.

Important chromosomal activities have been linked with both structural properties and spatial conformations of chromosomes. Local properties of the chromatin fiber influence gene expression, origin firing, and DNA repair [e.g., (*1*, *2*)]. Higher order structural features—such as formation of the 30-nm fiber, chromatin loops and axes, and interchromosomal connections—are important for chromosome morphogenesis and also have roles in gene expression and recombination. Activities such as transcription and timing of replication have been related to overall spatial nuclear disposition of different regions and their relationships to the nuclear envelope [e.g., (*3*–*6*)]. At each of these levels, chromosome organization is highly dynamic, varying both during the cell cycle and among different cell types.

Analysis of chromosome conformation is complicated by technical limitations. Electron microscopy, while affording high resolution, is laborious and not easily applicable to studies of specific loci. Light microscopy affords a resolution of 100 to 200 nm at best, which is insufficient to define chromosome conformation. DNA binding proteins fused to green fluorescent protein permit visualization of individual loci, but only a few positions can be examined simultaneously. Multiple loci can be visualized with fluorescence in situ hybridization (FISH), but this requires severe treatment that may affect chromosome organization.

We developed a high-throughput methodology, Chromosome Conformation Capture (3C), which can be used to analyze the overall spatial organization of chromosomes and to investigate their physical properties at high resolution. The principle of our approach is outlined in Fig. 1A (*7*). Intact nuclei are isolated (*8*) and subjected to formaldehyde fixation, which cross-links proteins to other proteins and to DNA. The overall result is cross-linking of physically touching segments throughout the genome via contacts between their DNA-bound proteins. The relative frequencies with which different sites have become cross-linked are then determined. Analysis of genome-wide interaction frequencies provides information about general nuclear organization as well as physical properties and conformations of chromosomes. We have used intact yeast nuclei for all experiments. Although the method can be performed using intact cells, the signals are considerably lower, making quantification difficult (*9*). The general nuclear organization of purified nuclei is largely intact, as shown below.

For quantification of cross-linking frequencies, cross-linked DNA is digested with a restriction enzyme and then subjected to ligation at very low DNA concentration. Under such conditions, ligation of cross-linked fragments, which is intramolecular, is strongly favored over ligation of random fragments, which is intermolecular. Cross-linking is then reversed and individual ligation products are detected and quantified by the polymerase chain reaction (PCR) using locus-specific primers. Control template is generated in which all possible ligation products are present in equal abundance (*7*). The cross-linking frequency (X) of two specific loci is determined by quantitative PCR reactions using control and cross-linked templates, and X is expressed as the ratio of the amount of product obtained using the cross-linked template to the amount of product obtained with the control template (Fig. 1B). X should be directly proportional to the frequency with which the two corresponding genomic sites interact (*10*).

Control experiments show that formation of ligation products is strictly dependent on both ligation and cross-linking (Fig. 1C). In general, X decreases with increasing separation distance in kb along chromosome III ("genomic site separation"). Cross-linking frequencies for both the left telomere and the centromere of chromosome III with each of 12 other positions along that same chromosome (Fig. 1, C and D) were determined using nuclei isolated from exponentially growing haploid cells. Interestingly, the two telomeres of chromosome III interact more frequently than predicted from their genomic site separation, which suggests that the chromosome ends are in close spatial proximity. This is expected because yeast telomeres are known to occur in clusters (*11*, *12*).

We next applied our method to an analysis of centromeres and of homologous chromosomes ("homologs") during meiosis in yeast (*7*). In mitotic and premeiotic cells, centromeres are clustered near the spindle pole body (*13*, *14*) and homologous chromosomes are loosely associated (*15*–*17*). These features change markedly when cells enter meiosis (*13*). The centromere cluster is rapidly lost and is not restored until just before the first meiotic division. Loose interactions be-

[1]Department of Molecular and Cellular Biology, Harvard University, Cambridge, MA 02138, USA. [2]Molekulare Genetik (H0700), Deutsches Krebsforschungszentrum, Im Neuenheimer Feld 280, and Kirchhoff-Institut für Physik, Physik Molekularbiologischer Prozesse, Universität Heidelberg, Schröderstrasse 90, D-69120 Heidelberg, Germany. [3]2e Oosterparklaan 272, 3544 AX Utrecht, Netherlands.

*To whom correspondence should be addressed. E-mail: jdekker@fas.harvard.edu